Heterogeneous Measurement System for Data Mining Robotic GMAW Weld Quality

This paper presents an integrated approach to these operations for a wide variety of weld data types and develops objective weld quality metrics

BY A. A. AYOADE AND J. P. H. STEELE

Abstract

During robotic welding, several streams of heterogeneous data can be collected. To gain a systemic understanding of the welding process, these data streams have to be combined precisely and accurately, especially if our goal is to develop online weld quality assessments. Establishing correspondence among temporal and spatially based data is a nontrivial effort. This article presents a data collection system using a novel methodology for establishing correspondence across multiple data sources of robotic gas metal arc welding for objective quality assessment. First, correspondence between the weld process data and the resulting weld required time synchronization and spatial alignment. Second, an objective weld quality extraction technique that assigns quantitative measures at a resolution of 1 mm of linear weld travel was developed to evaluate weld quality. Specifically, in addition to developing a method for objective weld profile assessment, we developed an objective analysis of radiographic data for the occurrence of subsurface porosity to assess defects and demonstrate how to objectively quantify the occurrence of surface porosity. While some aspects of this paper have been addressed individually and separately by other research, this paper presents an integrated approach to these operations for a wide variety of weld data types and develops objective weld quality metrics that can be used for machine learning of weld quality for robotic welding.

Keywords

- Weld Quality
- Heterogeneous Data Synchronization
- Image Analysis of Radiographic and Visual Images
- Machine Learning

Introduction

Data driven approaches to complex system understanding continue to demonstrate significant advances across a broad range of engineering applications. Because of the complexity of welding processes, the welding industry can benefit from these advancements and the development of future intelligent welding systems that control complex welding procedures to improve quality and reduce rejection rates.

Welding is essential in many important applications. From rockets and space travel to specialized instruments in medical applications, welding is a critical step in the manufacturing process and has been important to economic growth worldwide. By developing smarter robot welding units, more-intelligent process control, and automated quantitative quality inspections within the welding industry, significant productive improvements will be made in the future.

As sensor technologies improve and computational power increases, we want the welding robot system to become more intelligent. With the integration of machine learning tools, the goal is for the robot to become capable of recognizing abnormalities in the weld, identify the cause, and make immediate necessary corrective actions, leading to quality improvement without human intervention.

https://doi.org/10.29391/2022.101.008

Background: Gas Metal Arc Welding (GMAW) as a System

The welding process can be thought of as a sequence of three steps or stages. During each stage, different variables are controllable or observable. In the first stage, called the setup (or preweld) stage, parameter setting and system setup, like torch trajectory planning, contact-tip-to-work distance, gas composition and flow rate, wire size, and composition, are established. During the second stage, called the execution (or during welding) stage, the physical welding process is conducted and variables including arc current, arc voltage, travel speed, torch angle, cooling rate, heat and mass transfer, and other physical process variables are in play. The third stage, called the output (or postweld) stage, is characterized by the resulting physical weld and the corresponding characteristics, such as weld geometry, penetration, microstructure, mechanical properties, possible defects, and other resulting physical characteristics of the welding process. While most of the input variables are preset by a welding procedure, the execution variables vary depending on the physical realization of the process and the disturbances present and produce a weld with output characteristics that vary based on that manifestation. Given the temporal and spatial complexity of this multistage process, the requirements and challenges faced by a measurement system composed of several sensor technologies that must be synchronized to gather the process information from a subset of all the variables over all these stages are significant. In this work, while not all possible process information is included, we do include variable measurements from each stage of monitoring (setup, execution, and output) and show how to ensure that all the measurements are kept synchronized, irrespective of the signal type and source.

Online Weld Quality Prediction and Diagnosis

Each sensor technology carries with it advantages, challenges, and its applicability during or after the welding process. For example, inspection sensor technologies like radiography and ultrasonic sensing can provide subsurface information (e.g., porosity or slag) about the quality of the weld, while laser profiling and high-fidelity cameras can provide surface information about the quality of the weld (acceptable weld bead geometry), but they have corresponding issues regarding speed, time of evaluation (delayed evaluation or performed postprocess), cost, robustness, and accessibility, potentially limiting their usefulness for online quality assessment and diagnosis.

For a more flexible and accessible online solution, through-the-arc sensing is attractive since no additional hardware is required. This involves sensing the arc voltage and arc current that are in-process, real-time measurable, and fundamental components of the welding process. This makes them good quantities for obtaining patterns for diagnosing the process in real time and the occurrence of faults. Other real-time sensing capabilities can be added to measure quantities like temperature or acoustic signature of the process. However, these online sensing capabilities only directly measure the input and the intermediate variables of the process, which do not directly provide information about the quality of the weld. Thus, a form of mapping is always needed to determine weld quality.

To detect abnormalities and do diagnostics at the same time, one must fuse data from different sensor types, taking into consideration time disparities and spatial information and leveraging information from postprocess sensor technologies to develop an online in-process model for predicting weld quality and diagnosing the occurrence of faults in the process and defects in the welds. To achieve these goals, two tasks are required. The first task requires synchronization of a heterogeneous set of data from multiple sources, which will include but is not necessarily limited to voltage and current data from real-time sensors, weld quality information from the resulting weld bead profile and visual images, and postprocess x-ray radiographs. An appropriate implementation will involve both time synchronization and spatial alignment to synchronize both in-process and postprocess weld data. The second task requires an objective weld evaluation methodology to extract the weld quality information from the inspection sensors to supervise the mining of the data from the in-process sensors.

Details of these tasks are presented in this paper using the approach of a holistic measurement system. In the related work section, we review efforts to detect and document defects in gas metal arc welding (GMAW) processes. In the experimental procedures section, we describe in detail the system and methods used to collect weld data. In the data synchronization section, we show how data from a variety of heterogeneous sensors are synchronized, including images, robot pose information, and postweld radiographs. In the data analysis section, we discuss our technique for registering, analyzing, and quantifying the results from the x-ray radiographs. This allows us to resolve the occurrence and behavior of subsurface and surface defects at a resolution of 1 mm. In the discussion section, the benefits of this systemic approach to the data collection process are identified. Finally, conclusions are presented in the conclusion.

Related Work

Efforts to develop sensing systems to detect and correct defects in GMAW systems have been ongoing for more than 30 years. Sicard and Levine (Ref. 1) developed an overview of the system requirements for an intelligent adaptive robotic control system for GMAW and gas tungsten arc welding (GTAW) and discussed the visual imaging and thermal sensing requirements necessary to provide the needed information for the controller. Smartt et al. (Ref. 2) developed a monitoring system using dual cameras to measure the area to be filled and the temperature gradient in the solidified weld metal of a GMAW process. Using fuzzy logic, these data were used to determine the needed heat and mass input and appropriate cooling rate for the process.

A neural network mapped the requirements to welding parameters and travel speed. Quinn et al. (Ref. 3) developed a method of flaw detection for constant voltage GMAW using process voltage and current measurements. Algorithms were developed to assess weld quality, and another algorithm flagged the welds as matching previously identified good welds. Several defects were detected, including lack of shielding gas, oily parts, and melt-through, but the algorithm did not detect misalignment on 3-mm lap joints. On a production run, the algorithms were successful in identifying five out of six defects but missed small surface porosity (less than 3 mm). In a book edited by Zhang (Ref. 4), a number of sensor technologies for real-time process monitoring are presented as

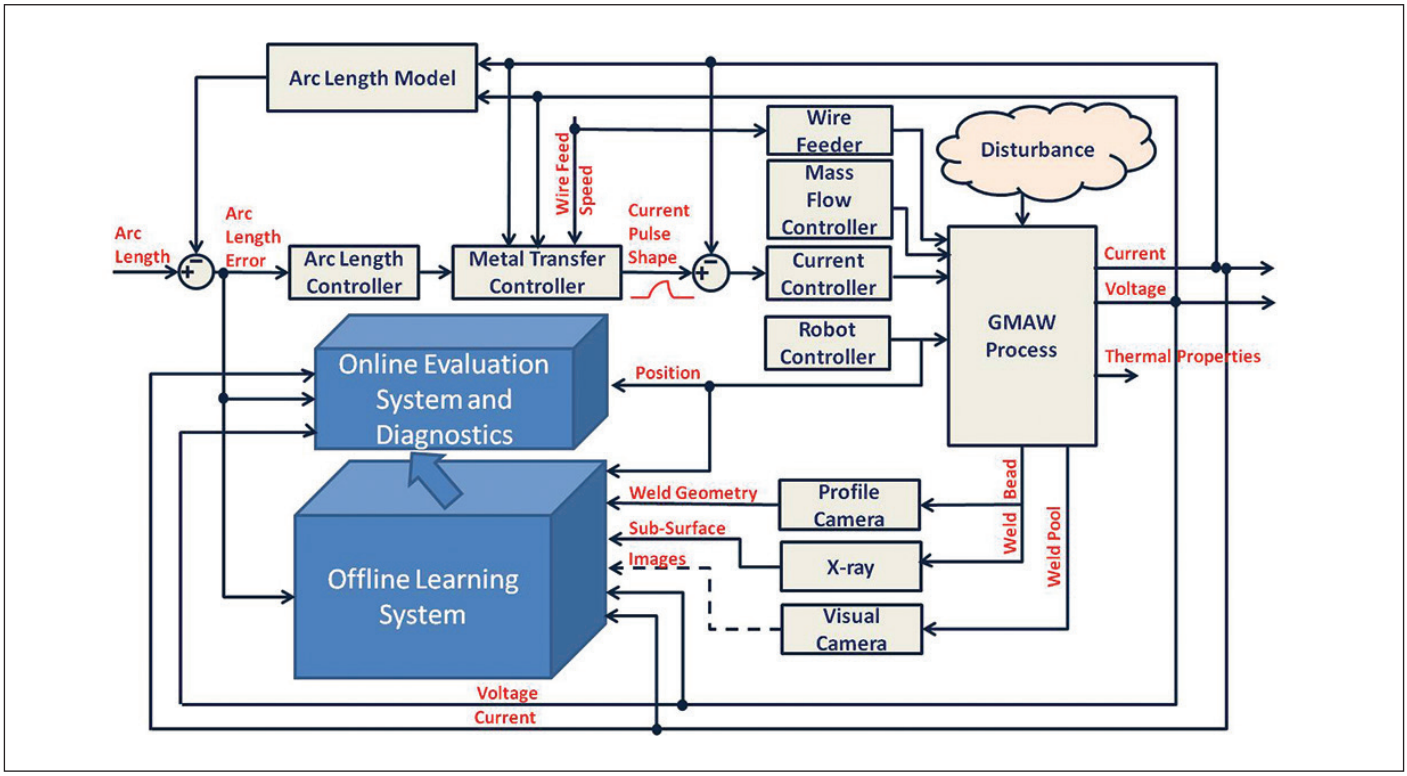

Fig. 1 — System block diagram.

well as chapters on monitoring various processes. Optical, infrared, and ultrasonic sensors are discussed and shown to provide separate contributions to real-time process monitoring. Wu et al. (Ref. 5) conducted through-the-arc, real-time sensing of voltage and current of a robotic constant voltage GMAW process on flat plate closed butt joint welds. Openings were cut into the root and represented step disturbances; thus, the location of the defect was previously known, so no data synchronization was required, and detection was predefined. Correlation of several statistical measures (mean, standard deviation, coefficient of variation, and kurtosis) to the weld quality were developed using statistical process control and a process control chart was developed, demonstrating how statistical process control for weld quality could be developed.

Zhang and Chen (Ref. 6) did multisensor fusion of arc light spectrum, arc sound pressure, and voltage signals of autogenous pulsed GTA welds with artificially introduced defects on plate butt joint welds. Signals were synchronized by collecting all the data on the same data acquisition (DAQ) computer. They note the light spectrum data were down sampled before being integrated into the data set. Spatial alignment of the data is presented but the precision of that alignment is not given. Fisher distance criterion was used for feature detection and support vector machines using cross validation were used to detect defects, but there was not quantification of the defects. Fan et al. (Ref. 7) state that "precision measurement of the weld pool surface characteristics is a bottleneck for accurate control of weld penetration as well as for successful development of [a] next-generation intelligent welding system." They provide an extensive history of vision research applied to weld pool monitoring and measurement. Yusof et al. (Ref. 8) collected acoustic signals obtained while GMAW on API 5L X70 gas pipeline steel and analyzed them using the Hilbert-Huang Transform to obtain the energy-frequency-distance plots that demonstrated strong correlation to areas of surface and subsurface porosity. Huang et al. (Ref. 9) used a spectrometer to monitor the arc spectrum while GTAW of aluminum to detect porosity. They used local linear embedding and empirical mode decomposition to reduce the spectral data to a spectral band of interest. An extreme learning neural network was then trained to identify large pore, small pore, and porosity free weld areas. With this information available, a fuzzy proportional-integral-derivative controller was developed to adjust the current of the GTAW process to respond to variations in butt joint weld opening and groove angle and reduce the occurrence of porosity. Zhang et al. (Ref. 10) provide a state-of-the-art review of welding manufacturing, including both GMAW and GTAW and other processes. They present a systems level approach to welding manufacturing, including modeling and control, and discuss advances in sensors for these control systems. In a follow-on article, Zhang et al. (Ref. 11) explore the use of machine learning and especially deep learning as it has been applied to welding. Cheng et al. (Ref. 12) provide a comprehensive literature review and analyses of the state-of-the-art of real-time sensing of GMAW and the mathematics for real-time control. They also discuss weld seam tracking and through-the-arc sensing.

In addition, much work has been done to develop and improve seam tracking systems (Refs. 13–21), measure weld profiles (Refs. 22–24), and, more recently, estimates of bead penetration (Ref. 25). While all these efforts involve gathering of weld process

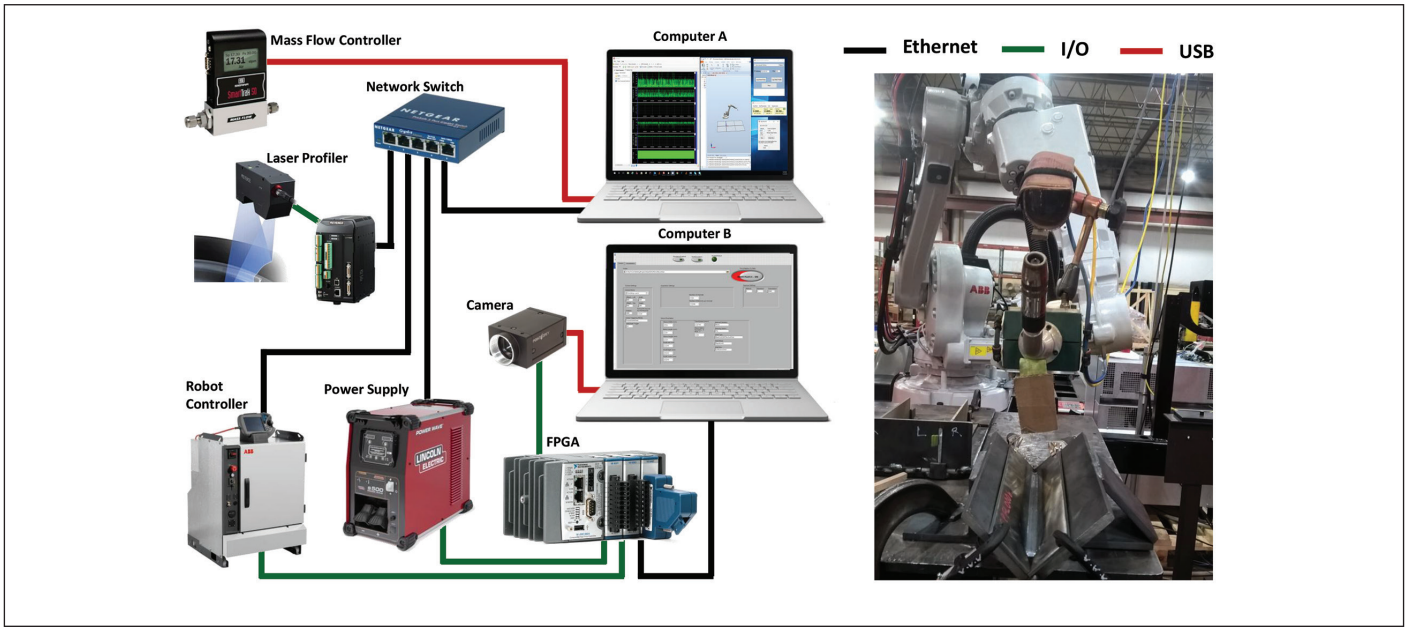

Fig. 2 — A multifaceted data acquisition system.

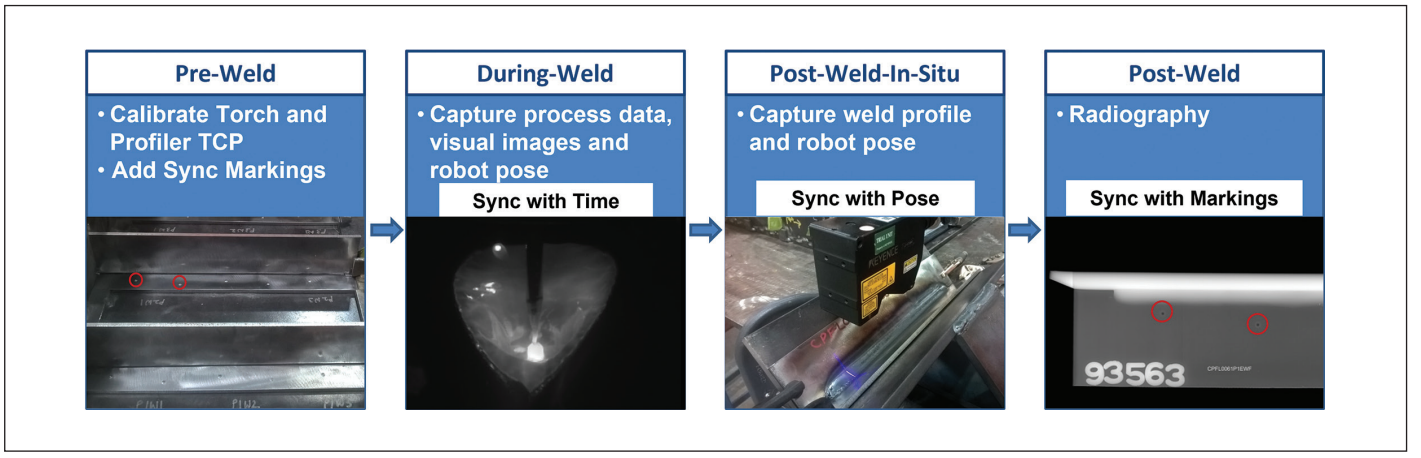

Fig. 3 — Data collection procedure.

data and collecting data from other components of the system, e.g., cameras, laser profilers, and robot controllers (robot pose information and torch travel speed), the degree to which these data are synchronized depends on the purpose of the work and the granularity of assessment desired. For example, if one simply wants to provide a good/bad weld assessment, identification of one qualifying defect is sufficient to classify the weld as bad, and no further information about weld process values or robot operational setting is needed. On the other hand, if we want to correlate the output characteristics at a particular location in the weld back to the weld process state at that point in time and place, then all the data that are relevant to the formation of the solidified weld at that specific location and time are needed to make a valid model and make an informed assessment. This necessarily implies that the data be synchronized both temporally and spatially. In the case of robotic welding applications, there is often a weave component included in the trajectory, and, perhaps, changes in torch and work angles. These must be accounted for if one is to fully represent the input data. So, except for specialized laboratory setups, the most reasonable approach for obtaining this information is from the robot motion controller. Thus, for more-detailed positional information about the electrode, especially when investigating different electrode orientations like work angles, travel angles, and motion patterns, it is better to use a robotic manipulator that is designed for this purpose. The challenge with industrial robotic controllers is that their positional information is not necessarily easily accessible. This challenge is often overlooked.

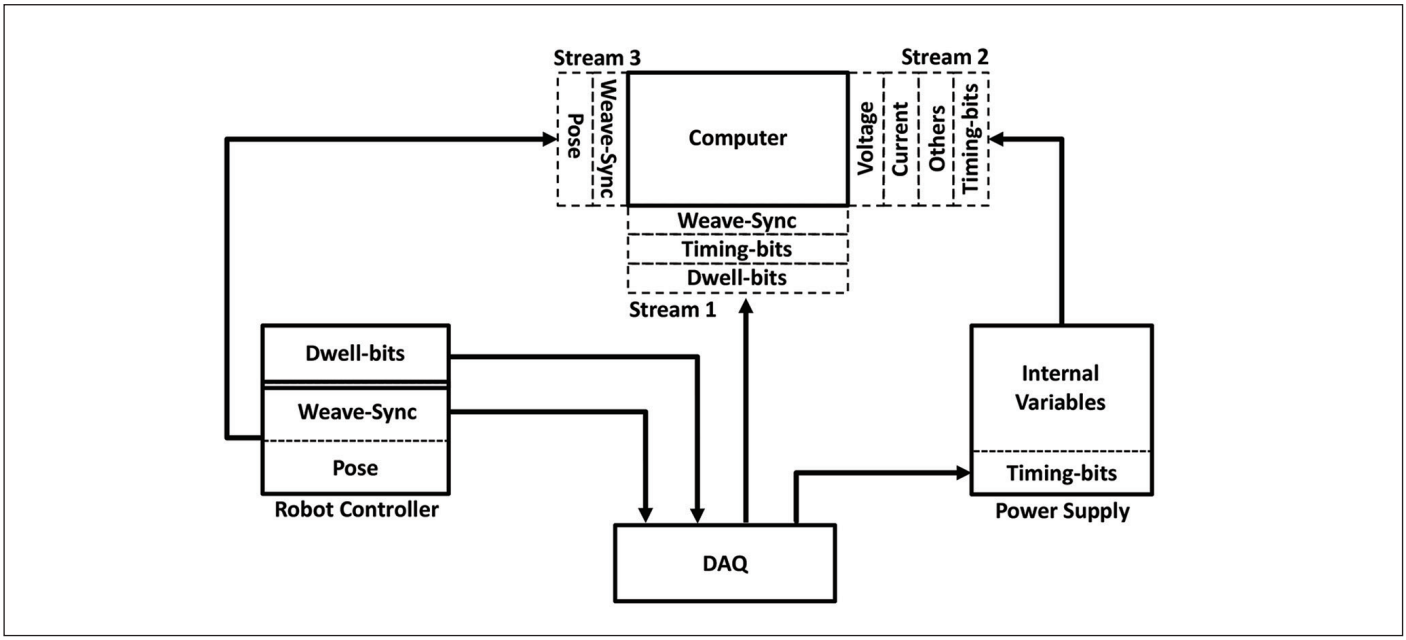

Fig. 4 — Time synchronization.

Purpose

The work presented here is an approach for developing a holistic systems-level methodology for dealing with heterogeneous data collection specifically for robotic GMAW that would be useful in other domains. Two specific challenges have been addressed that constitute the contributions of this work. The first challenge is the issue of temporal and corresponding spatial relationships for traditional robotic welding systems. Traditional robotic welding systems have separate proprietary controllers for the robot and for the welding unit. As we explain in the data synchronization section, the fusion of these data streams for external use is not directly available and requires the development of various software tools. The second specific challenge that must be faced is the correlation of time series data with the resulting weld bead profile (relevant to visual inspection), and, in our case, the correlation of x-ray radiographic images that are used to identify surface and subsurface defects, e.g., trapped slag, worm holes (trapped gas), and other irregularities (incomplete fusion). Thus, the approach presented in this paper integrates temporal and spatial data at a precision that allows for applying machine learning algorithms to investigate in-process predictors of weld quality at a multigranular level and make correlations back in time to all relevant data contributing to the formation of the solidified weld at specific points in space while leveraging objectively labeled data from postprocess sources.

Experimental Procedures

To acquire the needed data, one needs an acquisition system and a collection procedure that is flexible enough to handle data collection in-process and postprocess, knowing that all the data cannot be gathered simultaneously.

System Description

Figure 1 describes the system block diagram of an augmented robotic welding system equipped with sensors that capture both in-process data (i.e., voltage, current, arc length, electrode pose, and weld pool images) and postprocess data (i.e., profile, visual, and x-ray images of the weld bead) and how they all fit into an offline learning system to produce a model that captures the dynamics of the physical welding process and controller for online weld defect detection and diagnosis.

A photograph of the actual system assembly is shown in Fig. 2 alongside a diagram of the main subsystem devices. The system includes a Lincoln PowerWave® S500 with its built-in data acquisition system, an ABB IRB 1660ID robot, an AutoDrive® S wire feeder, a GS3-U3-23S6C Point Grey video camera, a SmartTrak® 50 mass flow controller, a National Instruments™ CompactRIO-9024 data acquisition system with its data acquisition modules, and a Keyence Model LJ-V7080 laser profiler. In the photograph in Fig. 2, the laser profiler can be seen below the torch, and the video camera is mounted behind the torch head.

Data Collection Procedures

Given the flexibility of data collection needed, in Fig. 3, we present a 4-stage sequential acquisition process with the following: 1) Setup stage that will be discussed later; 2) execution; 3) output/in-situ; and 4) output/postweld. These stages account for all the different ways sensors are used to measure data about a weld. Thus, this procedure can be modified to include other sensors in each stage. To keep each stage synchronized with the next stage, a sync marker is embedded during each stage of data acquisition. This is a major element of any successful heterogeneous data collection.

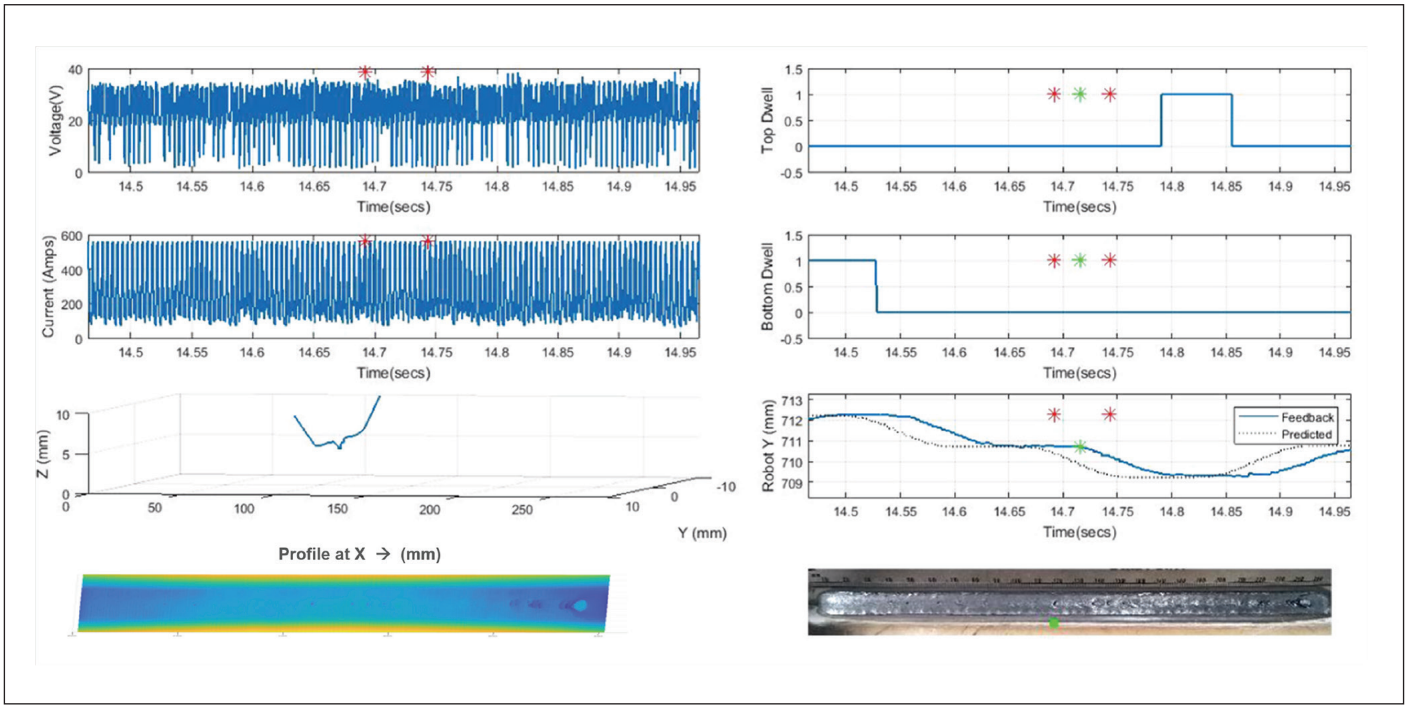

Fig. 5 — Synchronized in-process data with weld profile and weld visual photo.

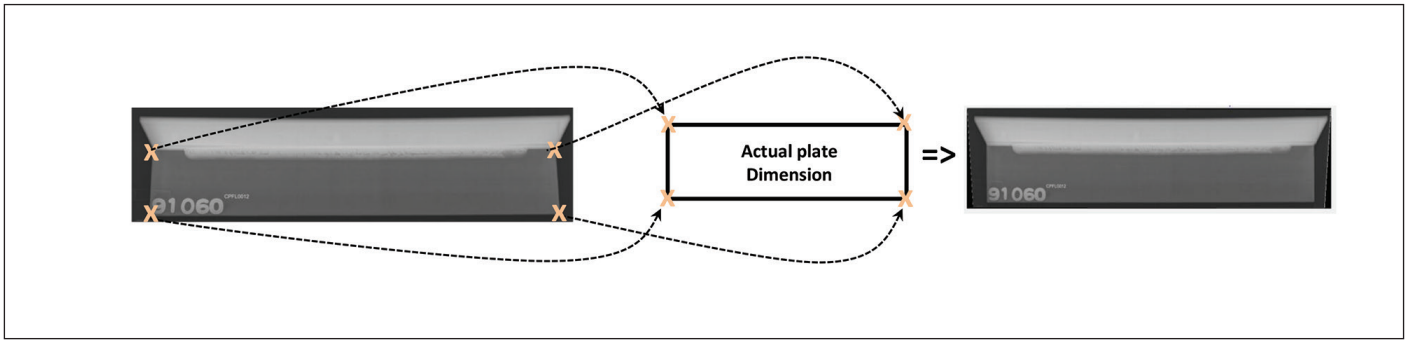

Fig. 6 — Mapping x-ray image to the actual plate dimension.

Setup/Preweld

During this stage of the process before welding, the tool center point (TCP) of the electrode on the welding torch is calibrated. Likewise, the TCP of the profiler camera is calibrated to have a reference point for overlaying postweld in-situ data measurements with the real-time online data acquisition. To ensure registration with radiographic images, the plates are physically marked with indents that are observable by the profiler camera and the x-ray machine.

Execution/During Welding

In-process (i.e., while welding), a synchronized measurement data collection of the voltage, current, arc length error, torch pose, and camera images are performed, synchronized in time by a systemwide timing signal of 1 kHz that is superimposed on each data stream source.

Output/In-Situ

After the weld is completed, any surface slag or spatter is removed from the weld bead. With the weldment still in position, the same path used during welding is retraced and weld-bead profile measurements are taken at 0.5-mm increments. At every measurement location, each profile captured is logged along with the full 6 deg-of-freedom pose of the robot.

Output/Postweld

In the final stage, the weldment is removed from the fixture and subsequently radiographed.

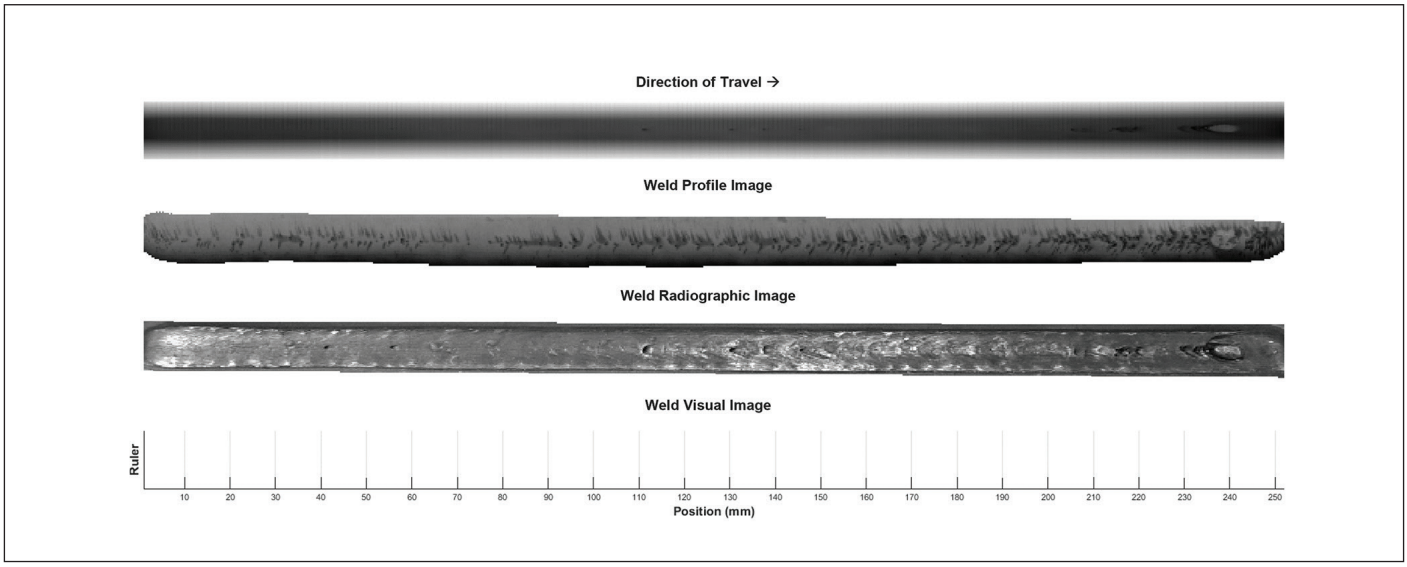

Fig. 7 — Spatial alignment of profile, radiographic, and visual images for a single weld run.

Results

Data Synchronization

In the previous section, we introduced the physical aspects (i.e., hardware, setup, and procedure) of creating the needed data. In this section, we discuss the internal workings of how synchronization is achieved. While external sensors can be used for in-process data measurements, modern power supplies and robots already possess many of the process variables of interest. For example, using the pose as provided by the robot is more direct than using other means. The challenge becomes time-synchronizing the two subsystems to gather already provided data alongside other external sensors. The electrode position can then be used to provide spatial alignment of the post-process weld quality data with the in-process time synchronized data.

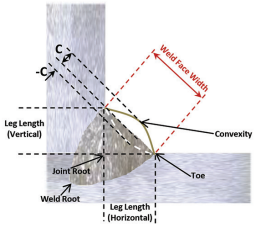

Width of Weld Face, W (mm)	Criteria	
	Min C (mm)	Max C (mm)
≤ 8.0	0	2.0
8.0 to 25.0	0	3.0
≥ 25.0	0	5.0

Fig. 8 — AWS D1.1 weld profile schedule.

In-Process Data (Time Synchronization)

This involves the synchronization of data provided by the power supply (process data), the robot (positional information of the electrode), and camera images. Synchronizing these devices is not as straightforward as one may think; they all use separate communication channels and are not generally built for this purpose. This is a challenge affecting the whole robotic welding industry. Hence, creativity and customization are required of these devices.

As seen in Fig. 4, the power supply and the robot controller send their data to a master acquisition device, a computer in this case, over separate channels, each with its own time stamp. This inherently comes with the problem of misalignment in the individual timing signals. By creating a central timing signal composed of a 1-kHz pulse stream, the power supply is synced with the DAQ computer, a NI CompactRIO-9024, by sampling these timing-bits at 120 kHz and overlaying them with the rest of the data available within the power supply. As for the robot controller, there is an internal restriction on adding timing-bits to the pose data. Instead, an internal sync signal called the weave-sync is added to the robot pose data, which changes state at the beginning of every welding procedure-segment during a weld run (with the constraint that each weld run must contain some amount of weave motion of the welding torch). The DAQ computer is then used to capture this weave-sync signal while simultaneously logging its own timing signal, which is the central timing signal. To handle latency, dwell-bits — a digital signal from the robot controller that indicates when the electrode is in the side wall with less than 1-ms latency — is also included. Adding these dwell-bits signals directly to the pose data would have been the easiest solution but is also not supported.

As shown in Fig. 4, we end up with three separate data streams coming into the computer, which are merged by upsampling to

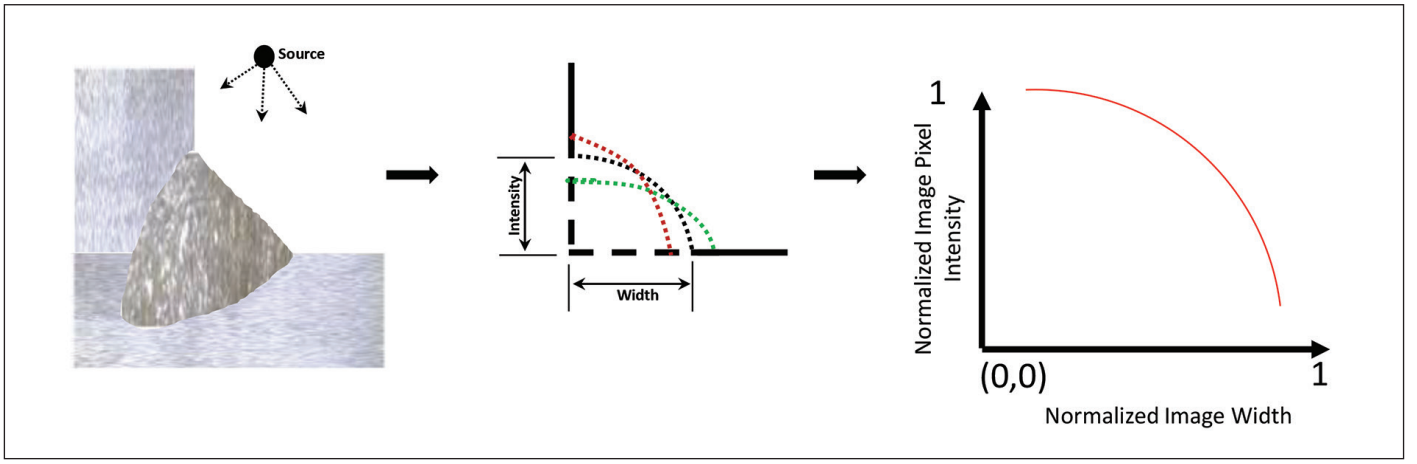

Fig. 9 — Normalizing the x-ray image pixel intensity and weld width.

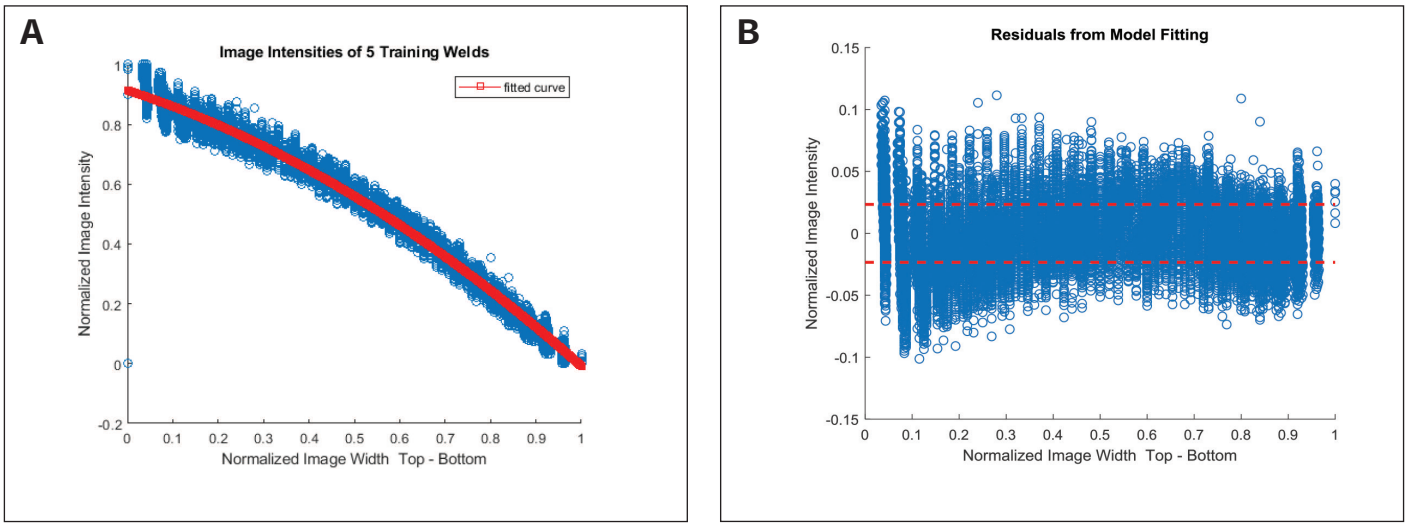

Fig. 10 — A — Fitting a quadratic curve to normalized pixel intensities of good welds; B — the residuals of the model with the two-standard deviation margin.

the same sampling frequency of 120 kHz. This includes Stream 1 from the DAQ computer, consisting of weave-sync, dwell-bits, and central timing-bits; Stream 2 from the power supply, containing the central timing-bits with voltage, current, arc length error, and other internal data; and finally, Stream 3 with weave-sync and pose data from the robot controller.

To minimize any latency to within 1 ms between the data stream from the robot controller and the DAQ central-timing bits, we isolate the robot pose data corresponding to a weave motion region using the start dwell-bit, the end dwell-bit, and the weave-sync state. The weave-sync state indicates the weaving region in the data while the start and end dwell-bits act as reference points for when the electrode was first in and last out of the side walls of the work piece. By computing the phase-shift in the robot pose data in its weaving axis with its mirrored version within these reference points, we could then reduce the latency to the 1-ms target. The 1 ms is a good resolution of time since the robot is traveling at 7.62 mm/s.

In most welding research test-beds, simple specialized mechanized systems are often used, thus making it possible to acquire the position of the electrode in addition to the process data using a single data acquisition system. In other research, positional information is either not acquired (or only approximated) or not needed. In our work, positional information is crucial, but its accessibility is limited by the available communication protocols and their associated latency. The time synchronization aspect of this approach is not new. However, by combining time synchronization with a latency reduction system allowed the gathering of a new set of weld data, synchronized precisely in ways people have not when approaching the problem of locating weld defects with high precision relative to the whole process data.

Figure 5 presents a 0.5-s snippet of the time synchronization output for a weld run. It contains the voltage, current, weld profile scan, weld profile image, dwell-bits, and electrode position within the weaving-axis of the robot as a function of time and includes an image of the resulting weld. The electrode position,

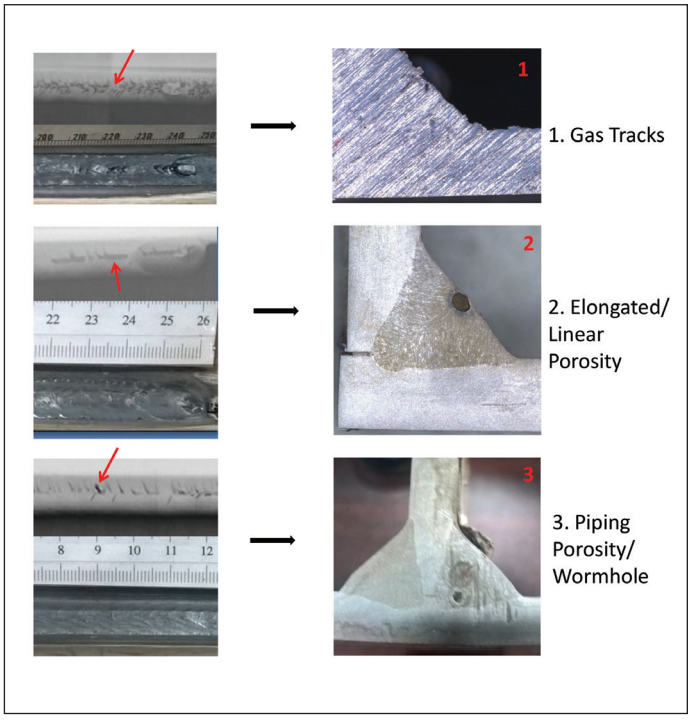

Fig. 11 — Macroevaluation of some welds with porosity.

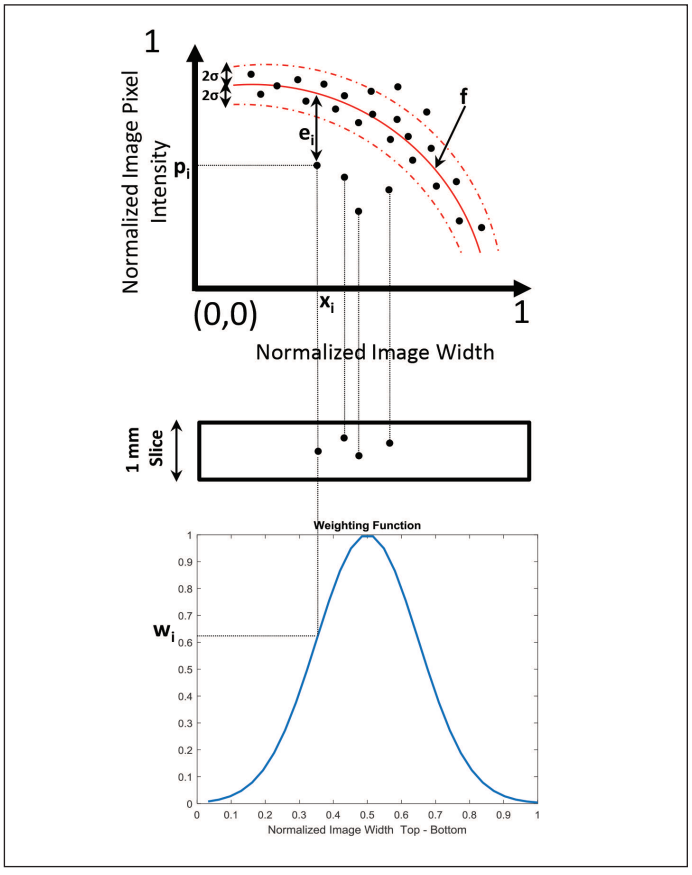

Fig. 12 — Finding outliers.

depicted with the green marker, corresponds to the weld profile scan (third image, left column) at that location in time. The dwell-bits are shown in the top two right side figures. The fillet weld was produced in the 2F position, i.e., one plate vertical and the other plate horizontal. The upper graph is for the vertical side and the second is for the bottom (flat) plate. The voltage and the current are the left side top two figures with the two red markers showing a window time of 66 msec that maps to the 0.5-mm weld profile scan interval when the electrode was at that location.

Postprocess Data (Spatial Alignment)

Since the positional information has been synchronized with the in-process data, all other data acquired postprocess can then be aligned provided they have the correct positional information. For the weld profile data, alignment is simple once the profile camera has been calibrated to have the same TCP as the electrode. Note that the positional repeatability of the ABB IRB 1660ID is 0.02 mm. By retracing the same programmed path used while welding, the pose data is acquired together with each cross-sectional profile scan of the weld.

The radiographic image is processed indirectly. As was shown in Fig. 5, we embed markers on the weld plates that reflect in both the radiographic image and the profile scans. Thus, we can align the radiographic image with the rest of the data by registering it with the profile image because the profile scans contain the positional information. By using these common features/embedded markers in both the weld profile image and the radiographic image with the actual dimension of the welding plate, a homographic transform is computed to register the images together. The steps to complete this are as follows:

1. Create an orthophotograph of the input image; in this case, the x-ray image. This is the correction of the camera angle from some off-axis pose so that the image is presented as if it were taken from directly overhead (Ref. 26). Using the edges of the bottom plate as control points, we calculate the transform between the actual plate dimensions and the x-ray image. This transform is then used to create a scaled orthoradiographic image, as shown in Fig. 6.

2. Calculate the homography transform between the weld profile image (in pixels) and the scaled orthoradiographic image above using the embedded markers/features common to both images. Using this transform, we can then map the positional information of the weld profile to the x-ray image.

3. Extract the weld region from the scaled orthoradiographic image with its corresponding positional information using active contour (Ref. 27). We can then evaluate this region for defects.

Using the same method, we can also add positional information to the weld photograph; that is, the visual image. An alignment of the weld profile image with the x-ray image and the weld photograph is shown in Fig. 7.

The surface appearance of the weld as well as evidence of the subsurface condition is shown. Additionally, the data necessary to determine the geometry of the weld bead is synchronized. With this alignment, we can provide an evaluation of the weld at any location desired, subject to the resolution of the profiler data, and match it to the corresponding process data. This provides significant benefits for the prediction of weld quality. However,

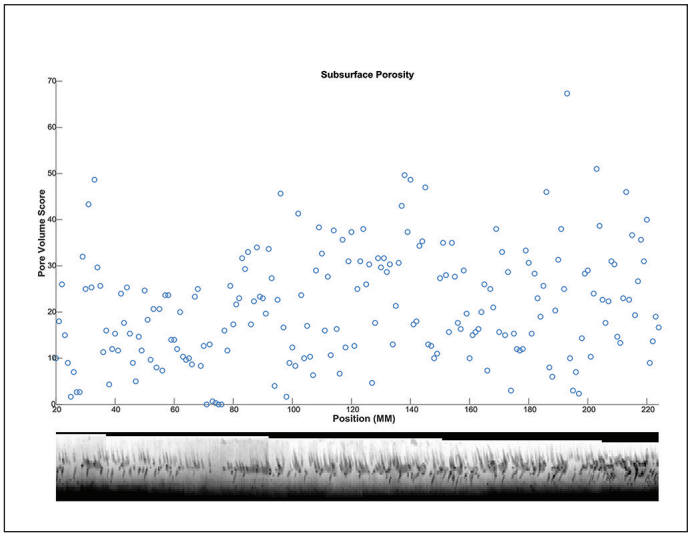

Fig. 13 — Subsurface evaluation of a radiographic image.

Fig. 14 — Step-by-step images of the surface evaluation process.

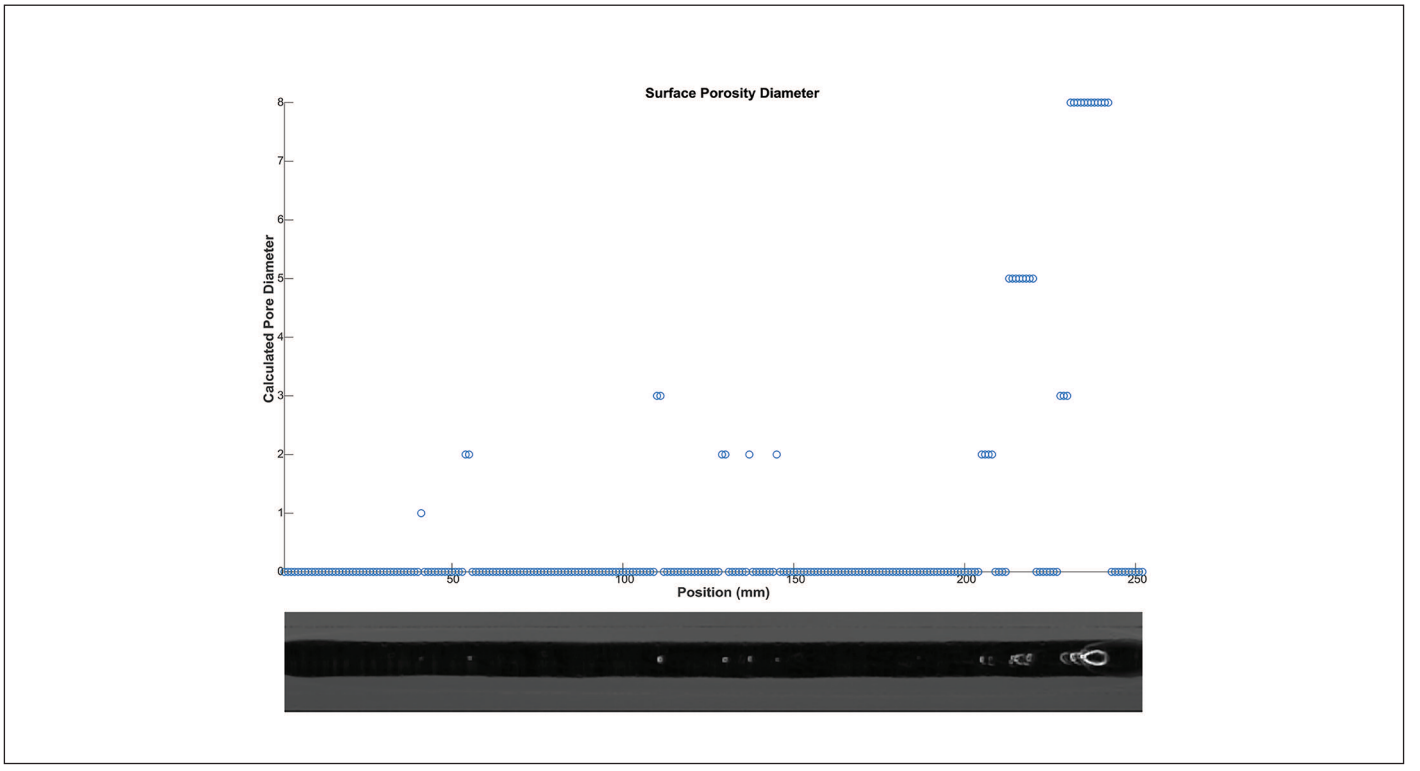

Fig. 15 — A surface evaluation for weld surface porosity measured in pore diameter.

these are just registered images. What is needed is actionable evaluation information for training learning systems. In the next section, we discuss an objective way to do this analysis using thresholds so that slices of the weld can be automatically labeled as defective or not.

Data Analysis

Quality assessment and acceptance labeling of the weld requires extraction of weld quality measures. While there are standards (e.g., AWS D1.1, *Structural Welding — Steel*) that specify threshold

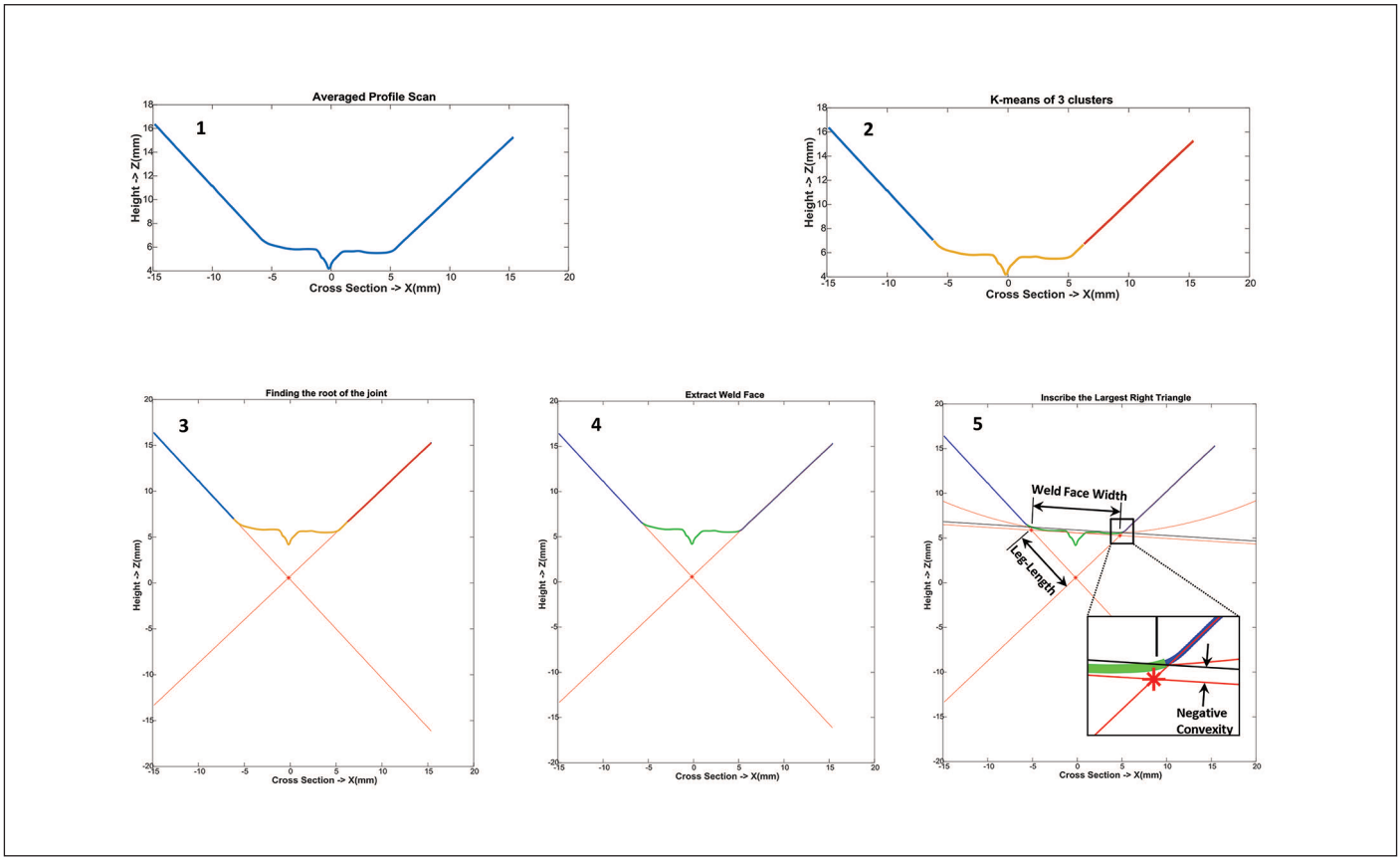

Fig. 16 — Graphical analysis of weld profile geometric properties.

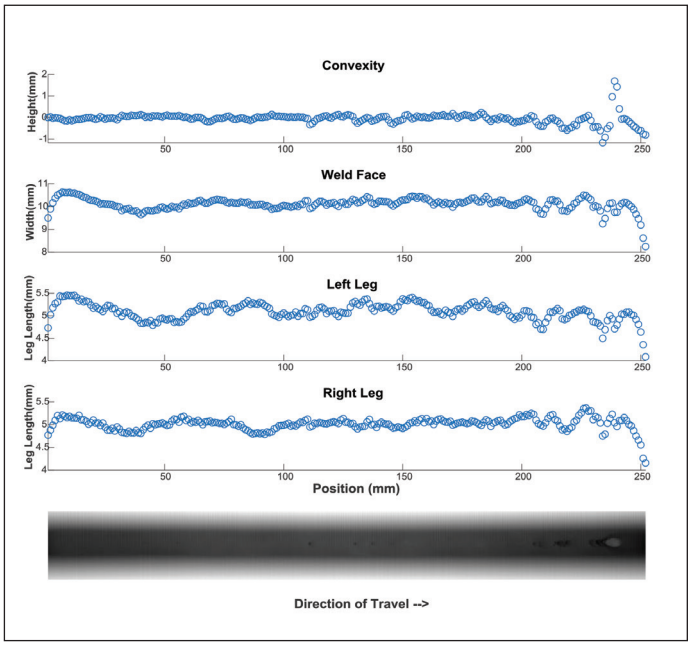

Fig. 17 — Extraction of convexity, weld face width, and left and right leg lengths from the geometric evaluation of the line scans from each 1-mm weld slice.

criteria for weld quality, human inspectors interpret these standards, and as a result, there is some subjectivity involved and uniformity of assessment cannot be guaranteed. In this section, we present objective evaluation techniques that allow automatic identification of defects with the flexibility to define thresholds for what should be considered acceptable or not in accordance with the requirements of the standards or project specific requirements. For a fillet weld, for example, AWS D1.1 specifies that the sum of the visible piping porosity 1 mm or greater in diameter shall not exceed 10 mm in any linear 25.4 mm of weld and shall not exceed 20 mm in any linear 300 mm length of weld. In addition, a table similar to Fig. 8 specifies the maximum convexity and concavity allowed for a given weld face width (provided the leg lengths meet the specified nominal dimension).

All these quantitative measures can be extracted from the sensor data and be used in combination with the standards. In this section, we describe methods for extracting relative subsurface porosity volume from radiographic images, surface porosity diameter from weld profile images, and other weld geometry information, including leg length, weld face width, and convexity measurements, from the profile scans. Rather than determining if the weld is acceptable or not as a whole, as in the standards, we extract this information at a resolution of 1 mm to understand how the quality of the weld is varying along its path.

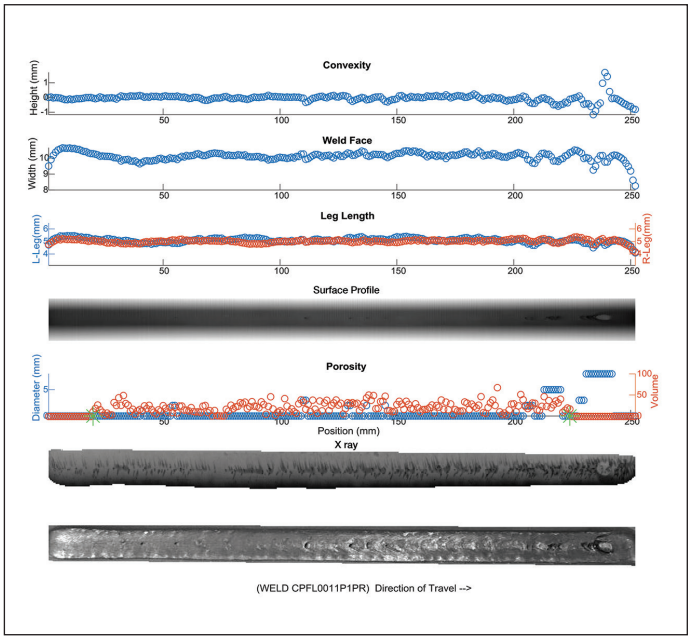

Fig. 18 — Sample #1: combined evaluation.

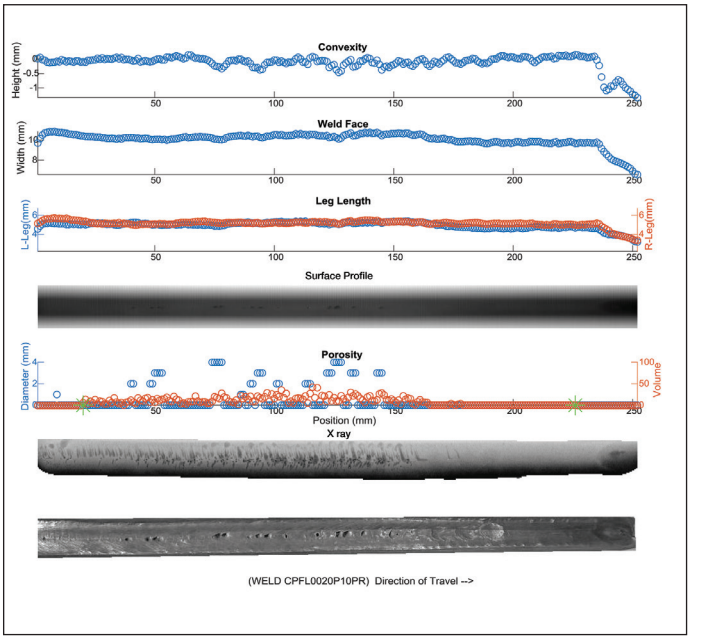

Fig. 19 — Sample #2: combined evaluation.

Subsurface Porosity Evaluation

Similar to certain aspects of other research (Refs. 28, 29), we perform background subtraction based on a model obtained from multiple normalized radiographic images of good welds. The idea is to capture a representative distribution (i.e., pixel intensities) of the surface of a good weld from one toe of the weld to the other and then find how the local distribution of other welds' pixel intensities deviate from this standard distribution.

The surface of the weld bead from the radiographic image can be modeled as a quadratic surface — Fig. 9. In the previous section, we discussed how to extract the x-ray of the weld bead from the radiographic image. However, the global pixel intensities of these images differ from one another depending on operators. Also, the width of the weld is not always the same depending on the positioning of the x-ray source relative to the plate, and the actual width of the weld bead. To avoid the effect of these variations, we normalize the segmented weld bead x-ray image in pixel intensity and weld width, as shown in Fig. 9, so that when the surface of any weld is modeled, we obtain normalized pixel intensities representative of the image densities of the weld bead from one weld to the other. In addition, the ends of the weld bead in the x-ray image are discarded to reduce the variability for these analyses.

To develop an exemplary distribution of the pixel intensities for good welds, normalized x-ray images of good welds are concatenated and fitted to a quadratic curve. From this quadratic curve, the residual, which is the deviation of each pixel intensity given its position across the normalized width of the weld from the quadratic curve, is computed. See Fig. 10 for an example of fitting five good welds. The variance, σ^2, of these residuals approximates the exemplary distribution that is needed for the evaluation of other welds.

The evaluation process is as follows: The aim is to compute a dimensionless measure that represents the volume of the pores buried in the weld at different locations along the weld at a resolution of 1 mm. Some macroevaluation examples of porous welds with their corresponding x-ray images are shown in Fig. 11. From these images, one can observe darker spots representing deeper voids along with some other not so dark but elongated areas along the weld. This means there is a relationship between the pixel intensity and the pore size and depth.

To capture this information in a form of pore volume at every slice of the weld, we apply the following algorithm:

1. Segment the weld region from the x-ray image and discard the ends of the weld.

2. Normalize the segmented weld region in pixel intensity and width.

3. Perform a local background subtraction (instead of a global one) to account for pixel intensity variation along the weld. That is, we fit a quadratic surface locally to an equivalent of 1-mm slices of the weld and then compute the residuals, $e_i = f(x_i) - p_i$, for each slice — Fig. 12. To reduce sensitivity to outliers, a robust least-squares method, least-absolute residuals that minimizes the absolute differences of the residuals rather than the squared difference is used.

4. Compute outliers. These are pixel intensities that fall below 2σ of the residuals of the training welds. Those above this threshold are ignored since they are not representative of pores in the weld.

$$d_i = \begin{cases} \frac{|e_i \cdot w_i| - 2\sigma}{\sigma}, & e_i \cdot w_i < -2\sigma \\ 0, & \text{otherwise.} \end{cases} \quad (1)$$

Note that the lower the pixel intensity, the darker the region. Since the image segmentation is not always exact at the edges of the weld region, a weighing function in the form of a normal distribution with its mean centered around the center of the weld region is introduced. This weight, w_i, takes into consideration the likelihood of a pixel being located within the weld bead and not just the plate.

5. Finally, compute the pore volume score, which is below,

$$pore\ volume\ score\ per\ slice = \frac{1}{M}\sum_{i}^{N} d_i \quad (2)$$

where M is the number of pixels per width of the weld slice and N is the total number of pixels within the slice. The distance, d_i, captures the depth of the pores as indicated by the pixel intensity, while the number of outlier pixels (i.e., with nonzero d_i) represents the area of the pore.

The result of an evaluation computed using this method is shown in Fig. 13. It shows a normalized image at the bottom of the figure and the corresponding scores at each 1-mm interval.

Surface Porosity Evaluation

We acknowledge the work done by Servo-Robot (Ref. 30) in identifying surface porosity and weld profile evaluation, but their work is proprietary. Here we present a simple, easy, fast, yet robust way to detect and measure the diameter of surface porosity in a weld. Image binarization is always tricky when working with images from visual cameras due to variations in light intensity. Realizing that images created by a laser profile camera are not affected by external light intensity, one can perform simple image binarization after performing some local filtering of the image. Steps are provided below. The resulting image after each step is shown in Fig. 14.

1. Transform the profile scan into an image while retaining the scaling.

2. Filter the image by computing the local standard deviation at every pixel location.

3. Binarize the image using Otsu's method (Ref. 31), which finds an intensity threshold that minimizes the intraclass variance between the two classes of white and black regions.

4. Finally, perform blob analysis on the image to extract the area of the white blobs. This is done by counting the number of pixels within that region. One can then compute the effective diameter in millimeters since the number of pixels per millimeter is known.

An evaluation result is shown in Fig. 15. It shows the computed diameter of each pore corresponding to its location along the weld. Note that the blob at the right of the weld is not really a surface pore but can be accounted for simply by only looking at blobs below the binarization threshold.

Geometric Evaluation

For a complete weld assessment, it is necessary to extract the geometric properties of the weld (e.g., width, length, and curvature). As one can imagine, this is based on quantifying lines and curves as presented in these articles (Refs. 32, 33, 34, 35). One main challenge here is performing these operations in a robust manner, especially in differentiating between the base plate and the face of the weld bead. Once this is accomplished, identifying defects is reasonably straightforward.

We apply the K-means clustering algorithm (Ref. 36) and the least absolute residual algorithm (Ref. 37) for line and curve fitting for this evaluation. After averaging the scans within the weld slice of interest, an approximate segmentation of the base plates from the weld face is found, as shown in the second plot in Fig. 16. This is done by clustering based on the cross-sectional distance and the height of the profile scan. The intersection of the fitted lines to these segmented scan points representing the left and right plates becomes the root of the joint, an important feature for computing the leg lengths (see Fig. 8). We then extract the weld face by finding the points when the scan points just curve away from the fitted lines, as shown in plot 4 of Fig. 16. The curvature of the weld can then be computed by fitting a quadratic curve to the weld face. To determine the leg lengths, we find the largest right angle triangle inscribed in the weld slice, ignoring the pore. That is, we are only considering the effective curvature of the weld. For convex welds, these are the intersections of the weld face curve with the fitted lines representing the weld plates. In the case of a concave weld, as shown in plot 5 of Fig. 16, the curve is offset by the height of the convexity, where the convexity is the distance between the maximum point on the weld face curvature and the line joining the toes of the weld. The sides of this triangle are then measured to denote the left and right leg lengths while the length of the hypotenuse of the triangle denotes the weld face width. An example of geometric evaluation for a complete weld is shown in Fig. 17.

Synchronized Weld Data Examples

To show how well the above algorithms work, we have shown two examples of a combined evaluation for two different welds in Figs. 18 and 19. The two green start markers denote the start and end of the evaluation for subsurface porosity. The top graph shows the measured convexity at each millimeter along the weld. The second graph shows the computed face width at 1-mm increments. The third graph shows the left-side leg length in blue and the right-side leg length in red in millimeters. The fourth graph is the surface profile laser scan. The fifth graph is the plot of surface pore diameter in millimeters in blue and the subsurface pore volume in red, again at 1-mm increments. The sixth graph is the x-ray of subsurface porosity. The seventh graph is a photo of the finished weld showing the profile and surface defects.

Both work pieces had been sprayed with a varying thickness of primer paint, and, as a result, both welds have significant amounts of subsurface porosity and several surface pores. Neither would be acceptable per D1.1. However, if one isolated their attention

to the last 50 mm of Fig. 19 for which data was collected, one will see a clean, acceptable weld. This being the last segment of the weld, it is suggested that a thinner layer of primer was applied, and because of the additional preheat time, the primer was vaporized off the workpiece.

We now focus our attention on features of Fig. 19. First, look at the bottom photograph that shows the surface of the physical weld. One can see a number of holes in the surface of the weld. If we look up two graphs to the porosity graph and the blue plot, we can see the alignment with the holes in the weld. The number of contiguous circles shows the breadth of these holes, and the height of the circles represents the diameter of these holes. This is clearly shown at about 75 mm with the dual pores with a diameter of 4 mm. We can count 13 surface pores. Turning to the red circles that represent the subsurface pores and wormholes, we see that there is essentially a continuous string of these pores from the beginning of the measure starting at 20 mm out to beyond 150 mm, the volume being larger in those regions with darker radiographic markings.

On the right-hand side of the weld beyond 175 mm, there is no surface or subsurface porosity. One can also see that the width of the weld is reduced by about 1 mm at this end of the weld by looking at the width of the weld face and by noting the leg length reduction in the left leg length in this good region of the weld. A similar analysis can be conducted on the other sample. All this data can be combined with the in-process data, voltage, current, travel speed, pose, and contact-tip-to-work distance to create an extensive model of the welding process and the resulting weld at a 1-mm resolution.

Discussion

Our focus is on the individual 1-mm data sets and the corresponding weld section result. By looking specifically at the input data for that slice and the corresponding output result, we can identify each as either passing or failing and label them as such. Using this microdefect labeling approach, we can build a data set that can be used to do machine learning.

To develop a deeper understanding of the relationship between weld process parameters, process variables, robot motion, and external influences, as well as their relationship to the resulting physical weld and weld defects, one must have access to a broad range of weld data from a variety of sensors and from postweld measurements and analyses that is fully synchronized. The system presented here provides that level of data integrity. In addition, a methodology for quantifying both surface and subsurface defects at the submillimeter level has been presented.

Effects of the Solidification Size of the Weld Pool

Since a weld pool takes time to solidify, a detailed data collection as presented in this paper can help to investigate the effects of temporal variations on defect formation. Such comprehensive heterogeneous data sets can also provide insights into defect diagnosis and prediction. We note here that we have previously indicated that data from several time steps are more appropriate to include in the input data, since defects such as subsurface and surface porosity take several sample periods to develop. A couple of ways to do this are to use recurrent neural networks (Ref. 38) or convolutional neural networks (Ref. 11).

Predicting Weld Quality at Various Levels of Resolution

Although a weld can be judged either good or bad simply by the presence or absence of defects globally, having a flexible quantitative measure allows one to determine at what level a defect predictor model is good at making predictions. The method developed here allows one to examine the quality of a weld at a fine resolution and to vary the resolution of such analyses. It also provides the capability of identifying correspondence between in-process variations of all sensed data and the occurrence of defects in the weld at a fine resolution, enhancing diagnosis.

Conclusions

This project demonstrates the challenge of aligning data for real-world applications of robotic GMAW and presents detailed methodologies for addressing those challenges. Major takeaways are as follows:

- A method for synchronizing and integrating process data and output data of various types at a resolution of 1 kHz and 1 mm spatially;
- A method for aligning surface scan data, weld photographs, and radiographs using a homographic transform;
- A method using a laser scanner to locate and size surface porosity; and
- A method for quantifying subsurface porosity using radiographic pixel intensity.

These tools will be necessary both for machine learning and for corrective control action and will be important for the development of the next generation of intelligent robotic welding systems.

Acknowledgment

This work was supported by Wolf Robotics, Fort Collins, Colo., and The Lincoln Electric Co., Cleveland, Ohio, under Grant 450467.

References

1. Sicard, P., and Levine, M. D. 1988. An approach to an expert robot welding system. *IEEE Transactions on Systems, Man, and Cybernetics* 18(2): 204–222. DOI: 10.1109/21.3461

2. Smartt, H. B., Johnson, J. A., and Einerson, C. 1993. The role of intelligent systems in weld process control. *Materials Evaluation* 51(10). OSTI Identifier: 5658229

3. Quinn, T. P., Smith, C., McCowan, C. N., Blachowiak, E., and Madigan, R. B. 1999. Arc sensing for defects in constant-voltage gas metal arc welding. *Welding Journal* 78(9): 322-s to 328-s.

4. Zhang, Y. 2008. *Real-Time Weld Process Monitoring*. Elsevier. ISBN: 9781845694401

5. Wu, C., Gao, J., and Hu, J. 2006. Real-time sensing and monitoring in robotic gas metal arc welding. *Measurement Science and Technology* 18(1): 303. DOI: 10.1088/0957-0233/18/1/037

6. Zhang, Z., and Chen, S. 2015. Data-driven feature selection for multisensory quality monitoring in arc welding. *Robotic Welding, Intelligence*

and Automation. Springer, pp. 401–410. DOI: 10.1007/978-3-319-18997-0_34

7. Fan, D., Zhang, G., Shi, Y., and Zhu, M. 2019. Progress and trend in intelligent sensing and control of weld pool in arc welding process. *Transactions on Intelligent Welding Manufacturing*. Springer, pp. 27–43. DOI: 10.1007/978-981-13-7418-0_2

8. Yusof, M., Kamaruzaman, M., Ishak, M., and Ghazali, M. 2017. Porosity detection by analyzing arc sound signal acquired during the welding process of gas pipeline steel. *The International Journal of Advanced Manufacturing Technology* 89(9–12): 3661–3670. DOI: 10.1007/s00170-016-9343-4

9. Huang, Y., Yuan, Y., Yang, L., Wu, D., and Chen, S. 2020. Real-time monitoring and control of porosity defects during arc welding of aluminum alloys. *Journal of Materials Processing Technology* 286: 116832. DOI: 10.1016/j.jmatprotec.2020.116832

10. Zhang, Y. M., Yang, Y. P., Zhang, W., and Na, S. J. 2020. Advanced welding manufacturing: A brief analysis and review of challenges and solutions. *J. Manuf. Sci. Eng. Trans*. 142(11). DOI: 10.1115/1.4047947

11. Zhang, Y., Wang, Q., and Liu, Y. 2021. Adaptive intelligent welding manufacturing. *Welding Journal* 100(1): 63-s to 83-s. DOI: 10.29391/2021.100.006

12. Cheng, Y., Yu, R., Zhou, Q., Chen, H., Yuan, W., and Zhang, Y. 2021. Real-time sensing of gas metal arc welding process — A literature review and analysis. *Journal of Manufacturing Processes* 70: 452–469. DOI: 10.1016/j.jmapro.2021.08.058

13. Bae, K.-Y., Lee, T.-H., and Ahn, K.-C. 2002. An optical sensing system for seam tracking and weld pool control in gas metal arc welding of steel pipe. *Journal of Materials Processing Technology* 120(1): 458–465. DOI: 10.1016/S0924-0136(01)01216-X

14. Xu, Y., Yu, H., Zhong, J., Lin, T., and Chen, S. 2012. Real-time image capturing and processing of seam and pool during robotic welding process. *Industrial Robot: An International Journal* 39(5): 513–523. DOI: 10.1108/01439911211249805

15. Ye, Z., Fang, G., Chen, S., and Dinham, M. 2013. A robust algorithm for weld seam extraction based on prior knowledge of weld seam. *Sensor Review* 33(2): 125–133. DOI: 10.1108/02602281311299662

16. Xu, Y., Lv, N., Han, Y., and Chen, S. 2016. Research on the key technology of vision sensor in robotic welding. *IEEE Workshop on Advanced Robotics and its Social Impacts (ARSO)*, pp. 121–125. DOI: 10.1109/ARSO.2016.7736268

17. Weis, A. A., Mor, J. L., Soares, L. B., Steffens, C. R., Drews-Jr, P. L. J., de Faria, M. F., Evald, P. J. D. O., Azzolin, R. Z., Filho, N. D., and Botelho, S. S. 2017. Automated seam tracking system based on passive monocular vision for automated linear robotic welding process. *IEEE 15th International Conference on Industrial Informatics (INDIN)*, pp. 305–310.

18. Zhang, Z., Wen, G., and Chen, S., 2018. On-line monitoring and defects detection of robotic arc welding: A review and future challenges. *Transactions on Intelligent Welding Manufacturing Vol. 2*. Eds. S. Chen, Y. Zhang, and Z. Feng. Springer, pp. 3–28. DOI: 10.1007/978-981-13-8668-8_1

19. Feng, Y., Chen, Z., Wang, D., Chen, J., and Feng, Z. 2020. Deep welding: A deep learning enhanced approach to GTAW using multisource sensing images. *IEEE Transactions on Industrial Informatics* 16(1): 465–474. DOI: 10.1109/TII.2019.2937563

20. Mann, S., Glebke, R., Kunze, I., Scheurenberg, D., Sharma, R., Reisgen, U., Wehrle, K., and Abel, D. 2020. Study on weld seam geometry control for connected gas metal arc welding systems. *IEEE 17th International Conference on Ubiquitous Robots (UR)*, 373–379. DOI: 10.1109/UR49135.2020.9144839

21. Sigüenza, M., Lean, P., and Cuellar, F. 2018. Design and development of a low cost hybrid sensor system for welding manufacturing. *IEEE 14th International Conference on Automation Science and Engineering (CASE)*, 574–579. DOI: 10.1109/COASE.2018.8560589

22. Xiong, J., and Zhang, G. 2013. Online measurement of bead geometry in GMAW-based additive manufacturing using passive vision. *Measurement Science and Technology* 24(11): 115103. DOI: 10.1088/0957-0233/24/11/115103

23. Rios-Cabrera, R., Morales-Diaz, A. B., Aviles-Vinas, J. F., and Lopez-Juarez, I. 2016. Robotic GMAW online learning: Issues and experiments. *The International Journal of Advanced Manufacturing Technology* 87(58): 2113–2134. DOI: 10.1007/s00170-016-8618-0

24. Pinto-Lopera, J. E., Motta, J. M., and Absi Alfaro, S. C. 2016. Real-time measurement of width and height of weld beads in GMAW processes. *Sensors* 16(9): 1500. DOI: 10.3390/s16091500

25. Yu, R., Han, J., Zhao, Z., and Bai, L. 2020. Real-time prediction of welding penetration mode and depth based on visual characteristics of weld pool in GMAW process. *IEEE Access* 8: 81564–81573. DOI: 10.3390/s16091500

26. Hoff, W. 2016. Computer vision, lecture notes. Colorado School of Mines.

27. Caselles, V., Kimmel, R., and Sapiro, G. 1995. Geodesic active contours. *Proceedings of IEEE International Conference on Computer Vision*, 694–699. DOI: 10.1109/ICCV.1995.466871

28. Wang, G., and Liao, T. W. 2002. Automatic identification of different types of welding defects in radiographic images. *NDT & E International* 35(8): 519–528. DOI: 10.1016/S0963-8695(02)00025-7

29. Chen, B., Fang, Z., Xia, Y., Zhang, L., Huang, Y., and Wang, L. 2018. Accurate defect detection via sparsity reconstruction for weld radiographs. *NDT & E International* 94: 62–69. DOI: 10.1016/j.ndteint.2017.11.006

30. Servo-Robot. 2021. Servo-Robot's automated weld inspection solutions. Retrieved November 17, 2021, from *servo-robot.com/servo-robots-automated-weld-inspection-solutions*.

31. Otsu, N. 1979. A threshold selection method from gray-level histograms. *IEEE Transactions on Systems, Man, and Cybernetics* 9(1): 62–66. DOI: 10.1109/TSMC.1979.4310076

32. Li, Y., Li, Y. F., Wang, Q. L., Xu, D., and Tan, M. 2010. Measurement and defect detection of the weld bead based on online vision inspection. *IEEE Transactions on Instrumentation and Measurement* 59(7): 1841–1849. DOI: 10.1109/TIM.2009.2028222

33. Chang, C.-L., and Chen, Y.-H. 2005. Measurements of fillet weld by 3D laser scanning system. *The International Journal of Advanced Manufacturing Technology* 25(5–6): 466–470.

34. White, R., Smith, J., and Lucas, J. 1994. Vision-based gauge for online weld profile metrology. *IEEE Proceedings-Science, Measurement and Technology* 141(6): 521–526.

35. Chu, H.-H., and Wang, Z.-Y. 2016. A vision-based system for post-welding quality measurement and defect detection. *The International Journal of Advanced Manufacturing Technology* 86(9–12): 3007–3014.

36. MacQueen, J. 1967. Some methods for classification and analysis of multivariate observations. *Proceedings of the 5th Berkeley Symposium on Mathematical Statistics and Probability, Vol. 1. Statistics*. Oakland, Calif., 281–297.

37. Barrodale, I., and Roberts, F. D. K. 1974. Solution of an overdetermined system of equations in the l1 norm [F4]. *Commun. ACM* 17(6): 319–320.

38. Elman, J. L. 1990. Finding structure in time. *Cognitive Science* 14(2): 179–211.

ADEWOLE A. AYOADE (*aayoade@mines.edu*) received his PhD in electrical engineering from Colorado School of Mines, Golden, Colo., and is now working at Lincoln Electric. **JOHN P. H. STEELE** (*jsteele@mines.edu*) is emeritus faculty and a research professor in mechanical engineering at the Colorado School of Mines, Golden, Colo.